Journal of The Electrochemical Society, **155** (10) D640-D650 (2008)
0013-4651/2008/155(10)/D640/11/$23.00 © The Electrochemical Society

QSPR Study of Passivation by Phenolic Compounds at Platinum and Boron-Doped Diamond Electrodes

Reinaldo F. Teófilo,[a] Rudolf Kiralj,[a] Helder J. Ceragioli,[b] Alfredo C. Peterlevitz,[b] Vitor Baranauskas,[b] Lauro T. Kubota,[a] and Márcia M. C. Ferreira[a,z]

[a]*Instituto de Química, Universidade Estadual de Campinas, 13084-971 Campinas, SP, Brazil*
[b]*Faculdade de Engenharia Elétrica e Computação, Universidade Estadual de Campinas, 13083-852 Campinas, SP, Brazil*

Blocking polycrystalline platinum (Pt) and boron-doped diamond (BDD) electrodes by 20 phenolic compounds was studied by means of chronoamperometric and theoretical methods [i.e., quantitative structure-property relationships (QSPRs)] and chemometric methods. The difference between the current densities after 15 and 90 s of oxidation time was proposed for the first time as a quantitative measurement of passivation on the electrodes. Structures of phenolic molecules and their hydrogen-bonding complexes with fluoride ion were modeled and geometry optimized with the B3LYP method and the 6-31G** basis set. Several molecular descriptors were calculated and correlated with the passivation measurements using the partial least-squares (PLS) regression method. A PLS model with one latent variable from five descriptors was built with high-level predictivity for phenolic passivation on the Pt electrode, and then was externally validated with four phenolics. The Pt model statistical parameters obtained were: $Q^2 = 0.786$, $R^2 = 0.851$, and standard error of validation (SEV) = 0.097. A BDD model with one latent variable and four descriptors was built and validated in the same way; however, the statistical parameters ($Q^2 = 0.333$, $R^2 = 0.586$, and SEV = 0.159) were of inferior quality with respect to the model for the Pt electrode. Both models were applied for prediction of 10 phenolic compounds. The Pt model showed to be suitable for predictive purposes. It was observed that passivation was much weaker on the BDD electrode than on the Pt electrode. Different interactions and reactions involving phenolics at the electrodes are the main reasons for such large differences between the models. Exploratory analyses were also performed and interpreted in terms of chemical concepts, such as phenolic reactivity, size/shape, hydrogen bonding, and electronic features. These findings can be useful to explore the possibility to predict phenolic passivation and to design electrochemical experiments involving different phenolic compounds. Furthermore, these PLS models aid in understanding electrode inactivation by phenolic compounds.
 [DOI: 10.1149/1.2953588]

Manuscript submitted January 29, 2008; revised manuscript received April 21, 2008. Published July 30, 2008.

It has been well known that phenols are readily oxidized in many chemical reactions and in electrochemical processes.[1-6] The obtained products are mostly mixtures of dimeric, polymeric, and quinone species.[1,4-7] The composition of such mixtures strongly depends on experimental conditions.[2,8,9] In electrochemical processes, the electro-oxidation of phenolic compounds begins with the formation of the phenoxyl radicals at solid electrodes and continues by two possible paths:[10,2] one pathway yields species with quinonic structure and the other one produces dimers and polymers. Some of these products are soluble and diffuse away from the surface, while others participate in the formation of an unreactive and impermeable polymeric film adhered on the electrode surface.[2,4-6,10] The phenomenon of formation of films on the electrode is known as passivation, poisoning, or fouling the electrode. Polymeric films represent a serious problem in electroanalysis (precision loss) and electrolysis (efficiency loss) of phenols because they cause rapid deactivation of the electrodes by blocking electron transfer and slowing down further oxidation.[2,4-7] In general, phenols are thermodynamically favorable for oxidative coupling,[1] and hence, all of them are able to form insoluble films on electrodes. Electrochemical polymerization, aside from its negative effects just described, has also received great attention because of some advantages in the use of aromatic amines to produce electroative and conducting polymer films,[11-13] and to protect electrodes against corrosion.[14,15]

Despite the great relevance of the phenol passivation process, in electroanalysis and in electrolysis, the formation and characteristics of the inhibitory polymeric film and the role of the operational conditions are not well understood. A better understanding of the phenol electropolymerization mechanism is of great interest from both the fundamental and practical viewpoints.[2]

General pathways for phenol electro-oxidation have been described by several authors.[5,16-18] The behavior of phenol during electro-oxidation may be considered as a general prototype for phenolics. Theoretical and experimental studies[4,19,20] have shown that the adsorption process occurs in two distinct and successive steps, as outlined in Fig. 1. The first one is the physical adsorption of the phenol oxygen followed by heterolytic scission of the O–H bond[21,22] and anion oxidation,[4,23] with the aromatic ring pointed toward the bulk of the solution (Fig. 1A and B). In the second step, the phenoxyl radical reorients from perpendicular (Fig. 1A and B) to a horizontal (Fig. 1C to F) configuration at the electrode surface, until the surface is fully covered by phenolic radicals.[19,20] In fact, the phenoxyl radical formed is the key intermediate in the phenolic electro-oxidation pathway. Its structure can be rationalized in terms of resonance forms, which explains how the radicals can combine to form different dimers. Such dimers, instead of oxidizing into quinone-like species, may, in turn, be oxidized at potentials lower than that of phenol to produce insoluble material radicals that can combine with another phenoxyl or dimer radicals to produce materials of high molar mass, a passivating ultrathin insulating film.[1,4,5,10] This radical coupling occurs at the electrode surface or in its immediate vicinity but not in the bulk solution.[24] The polymerization occurs mainly via "ortho" and "para" positions due to radical instability in these positions.[25] The presence of substituents on the phenol ring determines (*i*) whether the electropolymerization will be slower or faster relative to that for phenol, (*ii*) which intermediate phenoxyl radicals are more stable, (*iii*) which reaction products will be formed, and (*iv*) how they will be adsorbed at the electrode surface. This is because the products are usually kinetically and not thermodynamically controlled.[26] In fact, the pathway of this phenomenon is rather complex and may be affected by physical and chemical properties of the electrode material, solvent, pH, additives, concentration, and structural features of phenolic compounds, electrode potential, and current density, among others.[1-4,7,9,10,27,28] For instance, the formation of C–O bonds between radicals is favored in alkaline medium, whereas C–C bonds prevail in acid solutions.[5,17,29] Polymeric tar binding will also depend on the nature of the active groups present on the electrode surface and on the monocrystal or polycrystal structure of the surface.[8]

The majority of electropolymerization studies prioritize the analysis of the films obtained, but little attention is dedicated to the initial phenolic structures, i.e., the reactant monomers. Furthermore, quantitative data analyses on the passivation ability of different monomers are very scarce. The monomer structures as well as reac-

[z] E-mail: marcia@iqm.unicamp.br

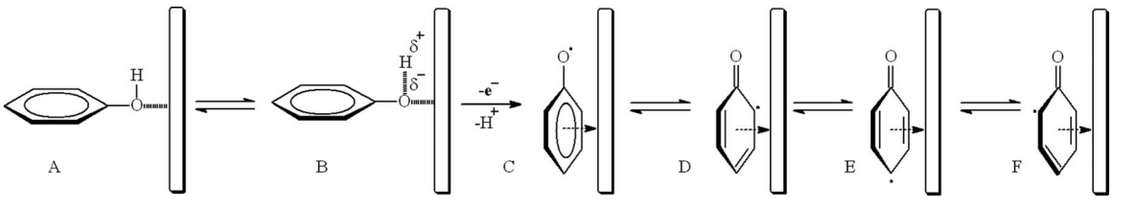

Figure 1. Mechanism of electro-oxidation of phenol.[19-23] Adsorption of phenol on an electrode (A–B), electro-oxidation (B–C), and resonance structures of the formed phenoxyl radical (C–F).

tivity, defined by the substituents at various substitution positions of the ring, will be responsible for the adhesion and permeability of the resulting polymeric film on the electrode. The deactivation ability of the polymer is directly related to its adhesion and permeability. Hence, a quantitative study on monomer structure and its passivation ability is desirable and can aid to understand the electropolymerization of phenolic compounds.

Computational chemistry approaches can be useful not only in understanding the electropolymerization phenomena but also in the prediction of the polymerization ability of a compound prior to experimental verification. Quantitative structure-activity relationship and quantitative structure-property relationship (QSPR) approaches are well-established methodologies that are useful in the prediction of various biological and physicochemical properties and chemical reactivity of substances for which there is no measured value yet of a property in question.[30] QSPR methods have been successfully used to predict several physicochemical properties. For instance, in two recent QSPR studies, the O–H bond dissociation energy for phenols was modeled using electronic properties of the substituents.[31,32] Furthermore, Nesmerak et al.[33] have presented a QSPR model to predict the substituent effects on half-wave potentials of benzoxazines.

In general, a QSPR analysis uses descriptors derived from the molecular structure. The advantage of this approach lies in the fact that the descriptors can be obtained computationally and are not dependent on carrying out experiments. Therefore, once a reliable regression model is established, it can be used to predict the studied property of new analogous compounds. Another advantage of QSPR studies is that they can show which structural features of the compounds play an important role in the modeled property. To the best of our knowledge, there is no QSPR work to predict electropassivation by phenols in the literature.

The purpose of this work is to establish parsimonious QSPR models that correlate molecular descriptors to the electrode fouling by phenolic compounds on platinum and boron-doped diamond (BDD) electrodes via partial least-squares (PLS) regression.[34,35] The models can give more insight into phenolic polymer formation at the molecular and even at mechanistic levels.

Experimental

BDD film deposition.— BDD films were produced as previously described using an all-quartz cylindrical hot-filament chemical vapor deposition reactor.[36,37] In summary, a boron-doping source was prepared by dissolving solid B_2O_3 in ethanol in a liquid reservoir before starting-up the reactor. Tungsten wires with diameter of 238 μm and length of 30 mm were used as substrates. The wires were mounted onto a polished silicon wafer placed below the hot filament, and parallel to the central axis of the filament coil. Deposition temperatures were measured by a thermocouple underneath the silicon wafer. Prior to deposition, the tungsten wires were dipped in a colloidal mixture of diamond dust (0.25 μm diam) dispersed by ultrasonic vibration in n-hexane. This "seeding" is a procedure used to increase the nucleation density of diamond films. The diamond films were deposited employing a mixture of ethanol vapor diluted in hydrogen gas (99.5 vol%) at a volumetric flow rate of 100 sccm/min, regulated by precision mass flow meters, and at a total pressure kept at 20 Torr. The boron-dopant concentrations estimated from Mott–Schottky plots were $\sim 10^{20}$ boron cm^{-3} (5000 ppm or 0.5% B/C). Electrical connections were placed on both types by wire wrapping a nickel-chromium wire and sealing with silver paint. The electrodes were insulated by a Teflon band and epoxy resin and then inserted into polypropylene tubes, exposing only the diamond area on the top of the electrodes for the electrochemical studies.

Several papers have shown that BDD electrode with a hydrogen-terminated surface is, generally, the most active and gives the most reproducible response.[36,38,39] Here, BDD films "as-grown" with very low quantities of nondiamond carbon phases on the surface received a mild cathodic treatment in 1.0 mol L^{-1} HNO_3. The cathodic treatment was carried out by cycling the potential in the range from 0 to − 4 V [vs saturated calomel electrode (SCE)] at least 3 times, according Teófilo et al.[36] This treatment likely hydrogenates the surface.[39] This pretreatment is also effective for recovery of diamond electrodes after extensive time use in analysis.

Voltammetry and chronoamperometry measurements.— An AUTOLAB PGSTAT-30 potentiostat was used to conduct electrochemical measurements. Polycrystalline platinum (Pt) wire (0.016 cm^2, geometric area) and a polycrystalline BDD (0.030 cm^2, geometric area) were used as working electrodes. All potentials were recorded against a SCE. The Pt electrode was polished before each measurement with 1 and 0.3 μm alumina powders slurried with ultrapure water (Milli-Q) on a microcloth polishing cloth followed by 5 min sonicating in alcoholic solution. The electrode was then rinsed with distilled water to eliminate any traces of alumina according to previously published procedures.[40,27,41] The BDD electrode received a mild cathodic treatment before any measurement, cycling the potential in the range from 0 to − 4 V (vs SCE) for at least 3 times in 1.0 mol L^{-1} HNO_3 under vigorous stirring.

The experimental study was carried out in a 5 mL cell using 0.05 mol L^{-1} phosphate buffer solution at pH 6.5 and a final concentration of 5.0×10^{-4} mol L^{-1} of phenolic compounds (from Sigma, Aldrich, Merck, Carlo Erba). All chemicals were of analytical grade and used without further purification. The solutions were prepared with ultrahigh purity water (MilliPore, Milli-Q system) or ethanol (Merck). The electrode potential was scanned in the range defined for each phenolic compound. The potential sweep rate was 100 mV s^{-1} at a step potential of 0.5 mV.

The electrochemical passivation was monitored using the chronoamperometric method. This method was selected due to its facility to fix the oxidation potential and to obtain information about electrode fouling at short times.[10] The potential was fixed at 50 mV more positive than the oxidation peak of a particular phenolic compound. The oxidation was carried out for 90 s, and the current was measured each 0.2 s (Fig. 2). The difference between the current densities after 15 and 90 s of oxidation time was defined as a parameter of passivation measurement on the Pt (Δj_{Pt}) and BDD (Δj_{BDD}) electrodes. This difference was selected inasmuch as the passivation was easily observed in the outset of the process. The chronoamperometric curves for the Pt electrode are presented in Fig. 2 for illustration. The measurements were carried out in triplicate, and the mean value was used for further data analyses. All experiments were performed at 25 ± 2°C. The studied phenolic compounds were catechol, chloroguaiacol, dopamine, guaiacol, hydro-

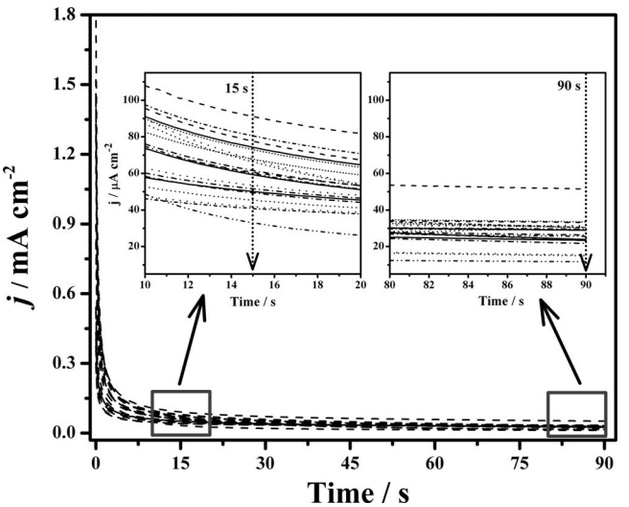

Figure 2. Passivation measured using chronoamperometric curves for the Pt electrode.

quinone, L-dopa, o-aminophenol, o-nitrophenol, p-aminophenol, paracetamol, phenol, resorcinol, serotonine, 5-hydroxyindole, o-cresol, p-chloro-m-cresol, m-cresol, p-cresol, o-chlorophenol, and L-tyrosine (Fig. 3).

Molecular modeling.— In order to model the molecular structures of the compounds studied, systematic searches were performed in the Cambridge Structural Database[42,43] via the ConQuest[44,45] searching interface and Mercury[44,46] and WebLab View Pro[47] visualization software. Experimental geometries of phenolic compounds or their analogues were obtained with the most probable O–H bond orientations. Whenever possible, internal hydrogen bonds were considered as stabilizing factors. Geometry optimization was performed at the density functional theory[48] (DFT) level with the B3LYP[49,50] functional and 6-31G** basis set within the framework of the Titan[51] molecular modeling software. A quantum chemical probe (fluoride ion) was used to simulate a strong hydrogen bond and changes in electron delocalization due to hydrogen removal. This simulation can provide information accounting for phenolic interaction with its chemical environment, including electrode, solvent, and other species. All modeled –OH…F complexes were geometry optimized at the same computational level as the phenolic molecules. Dihydroxybenzenes were modeled differently from the other phenols: only one OH group was hydrogen-bonded to the fluoride for the complex calculations. Compounds CATE, DOPA, and LDOP possess an internal hydrogen bond between the two neighboring OH groups. For such compounds, the OH group that acted as the hydrogen bond donor was modified by turning the O–H bond in the direction opposite to the other OH group to avoid the formation of a bifurcated hydrogen bond at the fluoride ion.

Various quantum chemical descriptors (independent variables) of steric and electronic nature were obtained from property calculations for phenolic molecules and their hydrogen complexes with the F^- ion by using the Titan software. Several compositional, topological, and steric descriptors for phenolic molecules were also obtained by using Dragon[52] software on the optimized geometries. Other compositional, topological, hydrogen bonding, electronic, and geometrical descriptors were calculated by which the total number of descriptors reached 700.

QSPR.— The calibration models were built using autoscaled molecular descriptors and the PLS regression method.[34,35] The input data for each PLS modeling were organized as a **X** matrix (descriptors data), where each row corresponded to a phenolic compound and each column to a molecular descriptor, and a **y** vector (dependent variable). The entries of **y** were the experimentally measured passivation abilities of the studied phenolic compounds, defined as the logarithms of the means $\log(\Delta j_{Pt})$ and $\log(\Delta j_{BDD})$ (in microamperes per centimeters squared) for the Pt and BDD electrode, respectively. The variable selection for both models was performed in two steps. In the first step, the correlation coefficients of **y** with all the descriptors were inspected and the cutoff of 0.50 and 0.40 was applied to the correlations relative to the Pt and BDD electrodes, respectively, by which the number of descriptors for building PLS models reduced to 30 and 13, respectively. In the second step, the variable selection was manually directed to satisfy several criteria: (*i*) satisfactory correlation with the passivation and acceptable PLS statistics (eliminating false nonlinearity, chance correlation, and pronounced nonuniform distribution or dispersion of points in the scatterograms), (*ii*) minimization of the number of high descriptor intercorrelations, (*iii*) selection of descriptors of different nature, calculation method, and clustering in hierarchical cluster analysis (HCA) and principal component analysis (PCA), (*iv*) computationally simple descriptors, and (*v*) chemically interpretable and under-

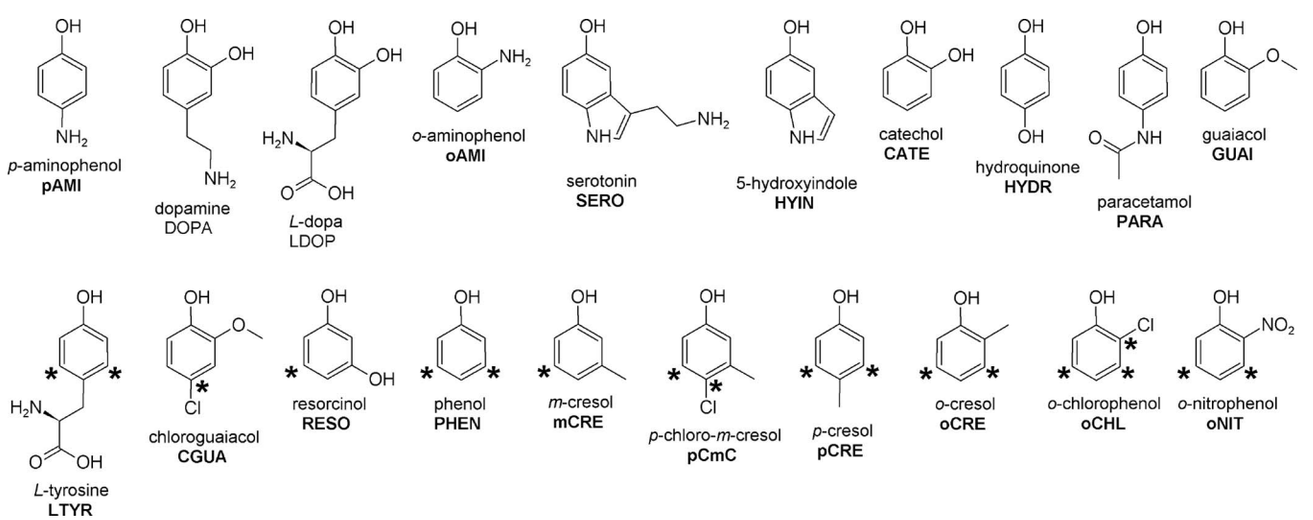

Figure 3. Structures of 20 phenolic compounds with measured passivation rates (training set), together with their names and the abbreviations used, and reactivity markers (sites for nucleophilic aromatic substitution).

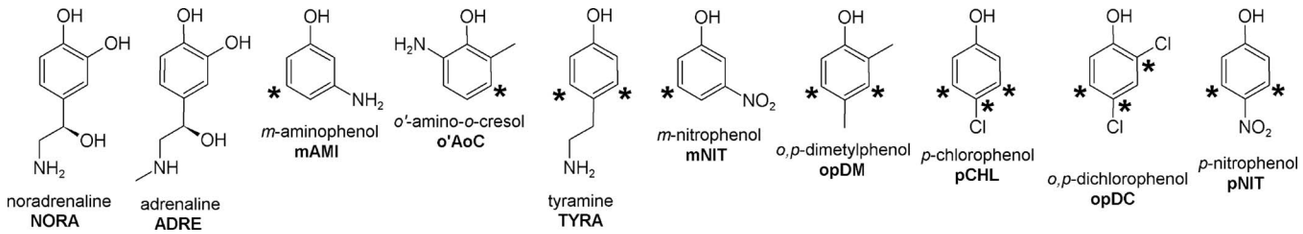

Figure 4. Structures of phenolic compounds without measured passivation rates (prediction set), together with their names and the abbreviations used, and reactivity markers (sites for nucleophilic aromatic substitution).

standable descriptors. After the correlation analysis (scatterograms and correlation coefficients), the following chemometric approaches for variable selection were used: leave-one-out cross-validation statistics, HCA dendrograms for descriptors, PCA loading plots, and regression vector components from PLS models.

The optimal number of latent variables in the PLS model was determined by two methods (i.e., leave-one-out cross validation and the recent randomization test proposed by Wiklund et al.[53]).

Two final PLS models were further validated by leave-*N*-out cross validation, where *N* varied from 1 to 8. The robustness of the models was tested by performing 10 *Y* randomizations according to Wold and Eriksson.[54] The original data were randomized prior to leave-*N*-out cross validation and *Y* randomization. The final validation procedure consisted of external validations, in which the original data sets were divided into as much as possible similar training (16 phenolics) and external (4 phenolics) validation sets with the aid of HCA.

HCA with incremental linkage and PCA of the two data sets that had been used in construction of the PLS models were performed in order to give deeper insight into the relationships between fouling and the electronic structure of phenolic compounds. The PLS models were used to predict the passivation power of 10 phenolics for which there were no experimental passivation data measured in the same conditions as for the 20 phenolics in this work (Fig. 4). The behavior of these phenolics at other platinum and carbon electrodes is known[55-61] and can be used for verification of the predictions.

All data analysis was performed using house-built Matlab-based functions in Matlab 6.5,[62] the Pirouette package,[63] and the algorithm for randomization test[53] available on the Web site http://www.chemometry.com.

Results and Discussion

Cyclic voltammetry and chronoamperometry.— Table I shows experimental results obtained for the phenolic compounds during their oxidation on the Pt and BDD electrodes using chronoamperometry. Phenolic oxidation on the Pt electrode is significantly different from that on the BDD electrode (Table I). It was noted that all phenolic compounds were characterized by higher peak potentials on the BDD electrode than on the Pt electrode. Oxidation at higher potentials indicates a low rate of electron transfer. This is in agreement with the literature, which reports relatively slow electrode kinetics as one of the reasons for lack of adsorption on diamond.[36,38,64,65]

The difference of current densities (Δj) obtained for the Pt electrode is significantly greater than that for the BDD electrode (Table I). The mean, standard deviation, and maximum and minimum values of Δj for the Pt electrode are 32.77, 14.10, 53.78, and 10.34 μA cm^{-2}, respectively. For the BDD electrode, these values are 12.91, 4.77, 21.65, and 2.99 μA cm^{-2}, respectively. These results indicate weaker fouling on the BDD electrode, which agrees with the literature reporting the characteristics of this electrode.[65,66]

Table I. Experimental results obtained using chronoamperometry for the Pt and BDD electrodes.[a]

	Pt				BDD			
Compound	j_{15}	j_{90}	Δj	$d\Delta j$	j_{15}	j_{90}	Δj	$d\Delta j$
PHEN	59.31	23.45	35.86	3.31	52.90	41.25	11.64	1.24
CATE	45.35	29.14	16.21	2.05	40.25	29.46	10.79	1.59
RESO	67.63	15.49	52.14	2.44	50.79	36.56	14.23	1.32
HYDR	53.63	30.69	22.94	0.41	39.02	27.72	11.31	2.42
oAMI	50.02	28.95	21.08	1.59	43.57	25.21	18.36	1.77
pAMI	41.84	31.49	10.34	2.85	34.65	26.50	8.14	1.48
PARA	60.62	33.17	27.45	0.49	43.22	30.32	12.90	3.56
oCRE	72.99	30.42	42.56	0.52	45.02	30.68	14.34	2.17
mCRE	66.29	15.05	51.24	0.65	56.67	35.02	21.65	4.80
pCRE	74.19	23.89	50.30	3.62	56.26	36.68	19.58	4.65
pCmC	61.58	21.73	39.85	0.39	30.64	24.53	6.11	2.94
oCHL	77.58	23.80	53.78	1.72	26.75	18.25	8.50	1.37
oNIT	80.45	30.45	50.01	5.29	39.99	27.83	12.17	1.06
GUAI	88.51	53.15	35.36	3.85	61.54	46.08	15.47	2.52
CGUA	67.79	33.52	34.26	1.61	32.35	22.99	9.36	2.43
LTYR	59.89	25.60	34.29	2.09	35.21	18.26	16.94	2.78
DOPA	40.82	29.20	11.62	1.13	33.55	30.56	2.99	0.50
LDOP	49.39	29.61	19.79	0.44	40.23	29.73	10.50	0.80
HYIN	33.00	11.80	21.21	2.10	58.55	39.27	19.28	3.07
SERO	51.57	26.37	25.20	1.91	26.77	12.92	13.85	1.28

[a] j_{15} and j_{90} (μA cm^{-2}): current densities obtained using the chronoamperometric time-current curve after 15 and 90 s, respectively; Δj (μA cm^{-2}): difference between j_{15} and j_{90}; $d\Delta j$: standard deviation differences from triplicate measures.

Table II. Molecular descriptors and passivations used in QSPR.

Compound	HBD/N	Mor06u	Qcnpa	Ar	QNUnpa	$\log(\Delta j_{pt})$	D-dCO/Å	DISPm	C-026	L(nCaH)	$\log(\Delta j_{BDD})$
PHEN	0.1429	−2	0.327	0.9993	−0.444	1.55	0.072	4	1	0.36	1.07
CATE	0.2500	−1	0.270	0.9965	0	1.21	0.078	5	2	0.16	1.03
RESO	0.2500	−1	0.342	0.9985	−0.206	1.72	0.073	3	2	0.16	1.15
HYDR	0.2500	−2	0.300	0.9994	0	1.36	0.074	0	2	0.16	1.05
oAMI	0.3750	−2	0.285	0.9944	0	1.32	0.072	2	2	0.16	1.26
pAMI	0.3750	−2	0.295	0.9773	0	1.01	0.073	3	2	0.16	0.91
PARA	0.1818	−2	0.313	0.9975	0	1.44	0.075	6	2	0.16	1.11
oCRE	0.1250	−1	0.332	0.9975	−0.451	1.63	0.075	2	1	0.16	1.16
mCRE	0.1250	−1	0.334	0.9990	−0.216	1.71	0.072	6	1	0.16	1.34
pCRE	0.1250	−1	0.321	0.9983	−0.437	1.70	0.073	5	1	0.16	1.29
pCmC	0.1111	−1	0.332	0.9977	−0.292	1.60	0.074	9	2	1.96	0.79
oCHL	0.1250	−1	0.315	0.9976	−0.577	1.73	0.080	9	2	0.16	0.93
oNIT	0.1000	−1	0.368	0.9994	−0.387	1.70	0.074	11	2	0.16	1.09
GUAI	0.1111	−1	0.296	0.9936	0	1.55	0.061	5	2	0.16	1.19
CGUA	0.1000	0	0.294	0.9925	−0.053	1.53	0.077	9	3	1.96	0.97
LTYR	0.3077	−2	0.271	0.9966	−0.445	1.54	0.086	10	2	0.16	1.23
DOPA	0.4545	−2	0.276	0.9903	0	1.07	0.089	3	2	1.96	0.48
LDOP	0.3571	−1	0.308	0.9835	0	1.30	0.075	7	1	1.96	1.02
HYIN	0.2000	−2	0.311	0.9803	0	1.33	0.072	2	1	0.36	1.29
SERO	0.3846	−2	0.327	0.9975	0	1.40	0.063	2	1	0.04	1.14
NORA	0.4167	−2	0.253	0.9958	0	—	0.090	9	2	0.36	—
ADRE	0.3077	−1	0.251	0.9947	0	—	0.086	15	2	0.36	—
mAMI	0.3750	−2	0.345	0.9971	−0.206	—	0.072	4	2	0.16	—
o'AoC	0.3333	−1	0.314	0.9949	−0.233	—	0.054	2	2	0.36	—
TYRA	0.3000	−2	0.323	0.9979	−0.434	—	0.074	9	1	0.16	—
mNIT	0.1000	−1	0.332	0.9982	−0.217	—	0.075	9	2	0.16	—
opDM	0.1111	−1	0.326	0.9976	−0.444	—	0.075	5	1	0.36	—
pCHL	0.1250	−1	0.325	0.9989	−0.542	—	0.074	9	2	0.36	—
opDC	0.1111	0	0.313	0.9972	−0.404	—	0.072	0	3	0.36	—
pNIT	0.1000	−1	0.357	0.9940	−0.393	—	0.079	6	2	0.16	—

It is worth indicating that, although there is a current decrease at the BDD electrode with time, the phenolic polymeric film formed is easily removed by stirring or, in worse situations, by performing a mild cathodic treatment under stirring.[36]

Molecular descriptors.— The final selected descriptors are presented in Table II, which also includes the dependent variables. No descriptor is common for the electrodes, indicating significant differences in electrochemical processes involving phenolic compounds at the two electrodes. The descriptors are described as follows:

1. Molecular descriptors related to phenolic passivation on the Pt electrode:

HBD/N, the number of acidic hydrogen atoms (related to hydrogen bond donors, HBD) divided by the number of nonhydrogen atoms (N), as obtained from the molecular formula

Mor06u, an unweighted 3D MoRSe signal 06 descriptor, a steric descriptor obtained using the Dragon software

Qcnpa, the (natural population analysis) NPA partial atomic charge of the phenolic carbon atom, which is chemically bound to the phenolic OH group, obtained from DFT computations for the isolated molecule

Ar, a modified Julg's aromaticity index[67] defined as $Ar = 255—(\sigma_b/d_b)^2$, where d_b is the average bond length and σ_b is the standard deviation of carbon-carbon bond lengths of the benzene ring, as obtained from the DFT geometry of the isolated molecule

QNUnpa, the sum of NPA atomic charges of phenolic carbon atoms, which are considered as formal sites for nucleophilic aromatic substitution. The value for this descriptor was set to zero when no sites of these kinds were identified. This descriptor is a reactivity index, which may be related, directly or indirectly, to the reactions between phenoxyl radicals. Interestingly, analog descriptors describing sites in electrophilic aromatic substitution were poorly correlated with the phenolic passivation on the Pt electrode.

2. Molecular descriptors related to phenolic passivation on the BDD electrode:

D-dCO, C–O bond shortening after the H…F hydrogen bond is formed, defined as the difference between the phenolic C–O bond lengths in the isolated molecule and the hydrogen bonded complex, as obtained from DFT calculations

DISPm, a dCOMMA2 value weighted by atomic masses, a conformationally dependent descriptor based on molecular geometry, as obtained using the Dragon sofware

C-026, the number of R–CH–R fragments, belonging to the Ghose–Crippen counts of atom-centered fragments, obtained using the Dragon sofware

L(nCaH), linearized form of nCaH, defined as $L(nCaH) = (nCaH–3.6)^2$, where nCaH is the number of unsubstituted aromatic Csp^2 atoms, a count of functional groups as obtained by using the Dragon sofware.

Charge analysis was performed for the phenolic carbon atoms to identify types of aromatic reactivity that would be related to phenolic fouling. In general, positions occupied by hydrogen atoms at the benzene ring can undergo electrophilic or nucleophilic aromatic substitution, while halogen atoms can be eliminated in a nucleophilic aromatic substitution. Phenols undergo radical-radical and even radical-anion reactions in which halogen atoms can be eliminated by the radical-nucleophilic mechanism $S_{NR}1$.[17] Ortho- and even para-, para′-positioned hydrogen atoms are substituted in phenolic radical-radical reactions.[6,17,29] Classical rules for strong, moderately strong, and weak ortho-para and meta orientations for elec-

Table III. Correlation matrix for dependent and independent variables used for QSPR.

Correlations between molecular descriptors

Descriptors for the Pt QSPR model

	Mor06u	Qcnpa	Ar	QNUnpa	$\log(\Delta j_{Pt})$
HBD/N	−0.579	−0.582	−0.425	0.525	−0.767
Mor06u	1.00	0.262	0.196	−0.238	0.558
Qcnpa		1.00	0.347	−0.686	0.777
Ar			1.00	−0.512	0.580
QNUnpa				1.00	−0.725

Descriptors for the BDD QSPR model

	DISPm	C-026	L(nCaH)	$\log(\Delta j_{BDD})$
D-dCO	0.305	0.316	0.579	−0.585
DISPm	1.00	0.348	0.408	−0.512
C-026		1.00	0.464	−0.509
L(nCaH)			1.00	−0.662

trophilic and nucleophilic substitution at the benzene ring[26,68] aided in identifying the sites for the two aromatic substitution mechanisms. A cutoff value of −0.24 in NPA charges for the phenolic carbon atoms was established, which enabled identification of the reaction site natures that could not be resolved by the classical rules. Nucleophilic substitution occurs when the carbon NPA charge is more positive than the cutoff, otherwise the site prefers electrophilic substitution. Figures 3 and 4 show the sites for radical-nucleophilic aromatic substitution in the phenolics studied in this work.

Correlation analysis (Table III) shows rather fair correlations between descriptors and the dependent variables (absolute values of correlation coefficients vary from 0.51 to 0.78), where there are low to moderate correlations between the descriptors (absolute correlation coefficients are in the range from 0.20 to 0.69). In the case of the BDD electrode, the descriptor-passivation correlations are somewhat smaller. This difference between the two electrodes is perhaps related to the fact that the electropassivation of the Pt electrode has been observed more intensely than that of the BDD electrode. Variable selection reconfirms these differences between the electrodes and between the corresponding electropassivation mechanisms (Table II). Although descriptors for the BDD electrode are predominantly steric/topological (only D-dCO contains some electronic effects), descriptors for the Pt electrode account for hydrogen bonding (HDB/N), electronic (Qcnpa, Ar and QNUnpa), and some steric (Mor06u) properties of the 20 phenols.

These facts can account for differences in electrode-phenolic interactions and chemical composition of the electroactive electrode surfaces. However, in the following, a more detailed inspection of the descriptor role is given.

The negative contribution of HBD/N to $\log(\Delta j_{Pt})$ means that a small number of polar hydrogen atoms is preferred for high passivation. Groups with polar hydrogens (from $-NH_2$, -NH, -OH and $-CO_2H$ groups, i.e., hydrogen bonding groups) can play several roles in phenolic passivation. They can participate in chemical reactions in which branched and less dense polymers are formed, because porosity is a general characteristic of phenolic polymeric films.[69] This includes formation of cavities filled with the solvent (water) and other species that interact with hydrogen bonding groups of the polymer. The hydrogen bonding groups can interact with the electrode surface or bulk solvent. These processes can slow down radical formation and the polymerization reaction, resulting in lower passivation.

The molecular shape descriptor Mor06u is related to steric aspects of phenolic polymerization. In general, more branched (less compact) molecules have smaller values of Mor06u, accounting for lower fouling. This situation is similar to that of the HBD/N, because more compact phenolic molecules will form denser polymeric films.

The increase of Qcnpa results in higher passivation. The more positive atomic charge of the carbon from phenolic C–OH means less negative charge at O (the two NPA charges are highly correlated for phenolic molecules, with a correlation coefficient 0.83). The descriptor Ar is an average measure of the benzene ring's aromaticity. The higher the ring's aromaticity (Ar) is, the higher the passivation is. Both Qcnpa and Ar are probably related to the chemical reactivity of phenolics, denser polymer packing, and perhaps to their interactions with the electrode.

QNUnpa (Table II), a quantum-chemical reactivity index, is directly related to the number of reaction sites for nucleophilic aromatic substitution (marked with asterisks in Fig. 3 and 4). The more negative the QNUnpa is, the higher the phenolic passivation via formation of a polymeric film on the Pt electrode is. This descriptor is related to the stability of intermediates in radical-mediated reactions. The first phenolic oxidation followed by radical formation is a crucial step for phenolic passivation. The radicals act like electrophiles by attacking substitution sites free for electrophilic aromatic substitution and also attack halogen-binding sites via the $S_{NR}1$ mechanism. Therefore, QNUnpa should be understood as an index showing how many sites undergo radical-electrophilic aromatic substitution (the sites not marked with asterisks in Fig. 3 and 4) and how many halogen-binding sites can suffer radical-nucleophilic substitution (the sites marked with asterisks in Fig. 3 and 4).

Descriptors for the BDD electrode can be also rationalized in a way similar to the descriptors for the Pt electrode, as follows. Fluoride ion, F^-, was used as a quantum chemical probe to simulate hydrogen bonding and electron withdrawal from and oxidation of phenolic compounds. The negative contribution of D-dCO to $\log(\Delta j_{BDD})$ can be interpreted as an external interference into the electronic structure of the phenolic molecule by means of intermolecular interactions or chemical reactions. Hydrogen withdrawal causes geometrical changes in the C–O group, visible as bond shortening due to the charge loss at O and stronger delocalization between the benzene ring and the CO group. Some phenolic molecules are more resistant to such changes due to the stability of the heteroaromatic system, so the corresponding D-dCO values are small.

Less flexible phenolics tend to form more homogeneous and denser polymeric films that are better absorbed at the electrode surface, as has already been noted from the Pt data set. This fact is visible from three descriptors. DISPm describes the conformational features of the phenolics. Low values of DISPm are expected for more rigid molecules that exhibit higher passivation due to the absence of long and flexible substituents and the presence of unsaturated bonds. C-026 shows that the absence of R-CX-R fragments (i.e., branching in the molecular structure results in higher passivation). The descriptor nCaH shows that the absence of substituted Csp^2 atoms in the structure favors passivation. Most compounds (16 of 20, with the exceptions being CGUA, DOPA, LDOP and SERO)

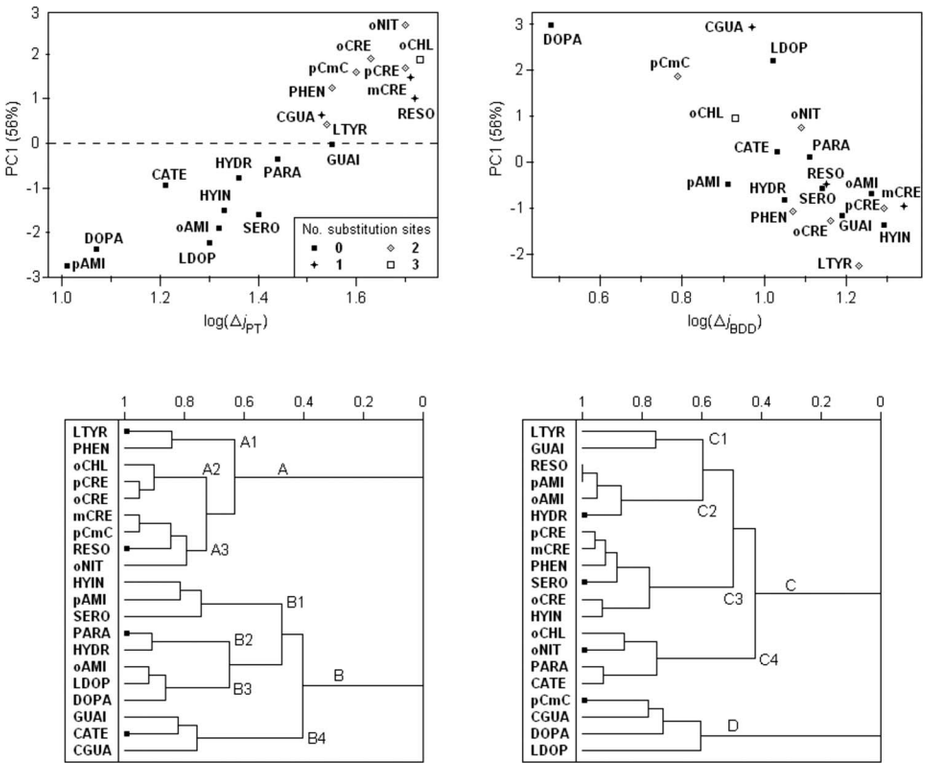

Figure 5. PC1 scores vs experimental $\log(\Delta j)$ plots (top images) and HCA dendrograms (bottom images) for molecular descriptors that were used to build the Pt model (left images) and the BDD model (right images). Compounds in the PCA-based plots are distinguished by the number of the most probable sites for nucleophilic aromatic substitution (zero and nonzero numbers are separated by the dashed line at PC1 = 0 for the Pt data set) and are arranged in the order of appearance along PC1 for the Pt data set. HCA subclusters are based on passivation and structural features of the compounds. Phenols that form external validation sets are marked with solid squares in the dendrograms.

show negative correlation between nCaH and $\log(\Delta j_{BDD})$. After transforming nCaH into L(nCaH), this trend is preserved.

Exploratory analysis.— Results of PCA and HCA for both data sets are shown in Fig. 5. These analyses give deeper insight into the nature of the molecular descriptors and their correlations with the dependent variables at the qualitative level. Molecular structures of the 20 phenolics in Fig. 3 are arranged exactly in the same order as the phenolics positioned along PC1 (from left to right) in the PCA plot for the Pt data set (Fig. 5, top left). This direction can be considered as increasing passivation, what can be easily verified by comparing the molecular structures (Fig. 3) and the experimental passivation data (Table I). The number of sites for nucleophilic aromatic substitution (derived from Fig. 3) can be zero (negative PC1) or can vary from 1 to 3 (PC1 is positive). These four groups of phenolics can be easily visualized in the scores plot, with an elevated tendency for nucleophilic substitution along PC1. When the same analysis of the scores plot for the BDD data (Fig. 5, top right) is performed, rather different and irregular trends in phenolic characterization can be observed. The passivation on the BDD electrode increases with the decrease in PC1, but the pattern of reactivity (number of substitution sites and corresponding charges) obviously does follow any other trend seen in the PCA plot for the Pt data. This, once again, reflects the rather different nature of phenolic-platinum and phenolic-diamond electrode interactions. It is interesting to note from PC1 vs $\log(\Delta j)$ plots (Fig. 5, top) good linear relationships between PC1 and experimental values of the dependent variable, with correlation coefficients of 0.921 and 0.765 for the Pt and BDD electrodes, respectively.

PC1 for the Pt and BDD data sets can be expressed by the following equations, where $[]_{au}$ denotes autoscaled forms of the original descriptors

$$\text{PC1} = -0.505[\text{HBD/N}]_{au} + 0.343[\text{Mor06u}]_{au} + 0.480[\text{Qcnpa}]_{au} + 0.393[\text{Ar}]_{au} - 0.492[\text{QNUnpa}]_{au} \quad [1]$$

$$\text{PC1} = 0.632[\text{DdC-O}]_{au} + 0.625[\text{DISPm}]_{au} + 0.382[\text{C-026}]_{au} - 0.253[\text{L(nCaH)}]_{au} \quad [2]$$

According to the nature and contribution of the descriptors in these expressions, the passivation process on the Pt electrode accounts for intermolecular interactions and chemical reactions that have 25% of hydrogen bonding character (HBD/N), 27% steric (Mor06u and Ar), and 47% electronic/reactivity nature (Qcnpa and QNUnpa). The same analysis for the BDD data points out mainly steric/geometrical (79%, DdC-O and DISPm) and compositional/topological [21%, C-026 and L(nCaH)] nature that determine interactions and reactions involving phenolics on the BDD electrode.

The HCA dendrograms consist of clusters, subclusters, and patterns that are well recognized. The dendrogram for the Pt data (Fig. 5, bottom left) consists of the clusters A and B, which correspond to the nonzero and zero numbers of substitution sites (see the corresponding PCA plot), with the exception of CGUA. This compound belongs to the B instead of the A cluster because it is the only phenolic with zero value of the descriptor Mor06u (Table II). It seems that the reactivity of the phenolic rings in this dendrogram is the main criterium for classification. This reactivity can be expressed in terms of ortho-/para- and meta-positioned substituents (activators or deactivators in nucleophilic aromatic substitution) besides the reference phenolic group, which depends on the nature of substituents, their position, and mutual interaction. All phenolics in cluster A have meta- and/or meta′-substitution sites and ortho/para-halogenated substitution sites (Fig. 2) relative to the reference phenolic group. Subcluster A1 is characterized with moderate passivation [$\log(\Delta j_{Pt}) = 1.54$–$1.55$] and is determined by electronic effects, whereas steric effects are not important. There are no substituents (activators or deactivators) in PHEN, and there is a weak activator in LTYR. Subclusters A2 and A3 consist of phenolics with high passivation (1.60–1.73). The phenolics in A2 possess a halogen and/or methyl that act as weak activators/deactivators. The phenolics in A3 contain weak deactivators and/or moderately strong to strong activators (oNIT). All the phenolics in cluster B contain some deactiva-

Table IV. Statistical parameters used for selecting the optimal number of latent variables for Pt and BDD PLS models: SEV values (leave one out), percent of variance, and risk of overfitting (in percent) estimated from 1000 randomization for individual latent variables.

	Pt			BDD		
LV	%Var	SEV	Risk	%Var	SEV	Risk
1	55.6	0.097	0.06	55.5	0.159	0.46
2	9.1	0.117	96.20	16.0	0.185	99.6
3	13.8	0.121	97.10	12.0	0.186	99.8
4	14.8	0.120	98.70	16.5	0.186	99.7

tors. Subclusters B1–B3 consist of phenolics with very low to moderate passivation (1.01–1.44) and which have strong ortho/para-placed deactivators (OH, NH_2, NHR): B1, with only para-activators (amino groups), B2 with para-OH/NHR, and B3 with ortho-/para-OH or NH_2. Sub-cluster B4 consists of phenolics with low to moderate passivation (1.21-1.55). These phenolics have a weak ortho-deactivator, with additional weak para-deactivator in CGUA.

The dendrogram for the BDD data (Fig. 5, bottom right) can be explained in terms of passivation ranges and some molecular features that are rather different from those for the Pt data set. Two simple properties can illustrate phenolic behavior at the BDD electrode: molecular topology expressed as the number of substituents on the phenolic ring (a fused heteroaromatic ring in SERO and HYIN is counted as one substituent), and average molecular polarity expressed as the C/X ratio (the number of carbon atoms divided by the number of X atoms, where X = O, N, and Cl). although phenolics in the C cluster range from low $[\log(\Delta j_{BDD}) = 0.93]$ to high (1.34) passivation and have at most one substituent, those in the D cluster have very low to low passivation (0.48–1.02) and two substituents. The latter compounds have $C/X \leqslant 3.5$, which makes them rather polar species. Among the C1–C4 subclusters, C3 is the only one containing phenolics with one or no (PHEN) substituent. These phenolics have moderate to high passivation (1.07–1.34) and $C/X > 3$ meaning that they are rather amphiphilic. Smaller ratios ($C/X = 3$) and a broad range of passivation (0.91–1.26) characterize subcluster C2. Although C1 subcluster has high passivation (1.19–1.23) and C4 has low passivation (0.93–1.11), both clusters are characterized by relatively high polarity ($C/X \leqslant 3$).

The BDD dendrogram points out possible interactions of a rather steric nature between the phenolics and the BDD electrode. There must be various types of putative interactions that depend on the structure of phenolic molecules and their size/shape properties. Lower branches and amphiphilicity are preferred phenolic molecular features and indicate the existence of limited domains or places of definite geometry to accommodate phenolic species at the BDD electrode, which agrees well with the findings of Chang et al.[70]

QSPR.— Statistics of the two PLS models are presented in Tables IV and V. Table IV shows statistical parameters used for the determination of the number of latent variables for the final PLS models. It is important to note that both methods, leave-one-out (Table V) and the randomization test[53] (Table IV), have indicated one latent variable (LV) for the Pt and BDD models. The risk of overfitting obtained from the randomization test is in excellent agreement with other parameters from leave-one-out cross validation (%Var and SEV). Good linear correlation between PC1 and experimental $\log(\Delta j)$ (Fig. 5, top) agrees with selection of LV1 for building PLS models for the Pt and DBB electrodes. The prediction power of the models is demonstrated in Table VI and Fig. 6, whereas leave-*N*-out cross validation and *Y* randomization of the models are presented in Fig. 7. Some statistical conditions, as defined by Tropsha et al.[71] and Golbraikh and Tropsha,[72] were applied to verify the prediction power of the models. These conditions include: (*i*) all correlation coefficients are $R^2 > 0.6$ and $Q^2 > 0.5$ for the training sets; (*ii*) the average Q^2 from leave-*N*-out cross validations must be high; (*iii*) the values R^2 and Q^2 from *Y* randomizations must be small. The Pt model well satisfies all these conditions, whereas the BDD model is shown to be weaker. Both models use only one latent variable describing 56% of the total variance. Most statistical parameters show that the Pt model is more reliable than the BDD model. Pronounced differences between the models are obvious from the correlation coefficients, especially Q^2 from various validation approaches, particularly from leave-*N*-out cross validation (Fig. 7, top). However, there was no chance correlation was found for both models (Fig. 7, bottom).

Table V. Comparison of the Pt and BDD PLS models with regression statistics.

Parameters	Pt model	BDD model
LV (%Var)[a]	1 (55.6%)	1 (55.5%)
SEV[b]	0.097	0.159
SEC[b]	0.086	0.132
Q^{2}[c]	0.786	0.333
R^{2}[c]	0.851	0.586
R.e. $\geqslant$ 10.00%[d]	3	8
Max. R.e.[d]	13.9%	60.4%
Mean R.e.[d]	5.1%	11.1%
Leave-*N*-out cross validation[e]		
$\langle Q^2_{LNO} \rangle$	0.795	0.350
Y-randomization[f]		
Q^2_{Yrand}	−0.058	−0.051
R^2_{Yrand}	0.281	0.326
External validation[g]		
SEV_{ev}	0.095	0.177
SEC_{ev}	0.080	0.140
Q^2_{ev}	0.807	0.245
R^2_{ev}	0.881	0.586
Regression vector	HBD/N: −0.276	DdC-O: −0.263
	Mor06u: 0.201	DISPm: −0.230
	Qcnpa: 0.279	C-026: −0.229
	Ar: 0.208	L(nCaH): −0.298
	QNUnpa: −0.261	

[a] Number of latent variables used and the corresponding percent variance of the **X** data matrix.
[b] Standard deviations of the PLS model: SEV—standard error of leave-one-out cross validation, SEC—standard error of calibration.
[c] Squares of correlation coefficients of the PLS model: Q^2—correlation coefficient of leave-one-out cross validation, R^2—correlation coefficient of calibration.
[d] Relative errors: R.e. $\geqslant$ 10.00%-number of phenolics with relative error $\geqslant$10.00%, Max R.e.—maximum relative error, Mean R.e.—mean relative error.
[e] Average Q^2 correlation coefficient of leave-*N*-out cross validations where $N = 1,2, \ldots ,8$.
[f] Maximum Q^2 and R^2 correlation coefficients of 10 *Y* randomizations.
[g] Common parameters for the training set in external validation test: SEV_{ev}—standard error of leave-one-out cross validation, SEC_{ev}—standard error of calibration, Q^2_{ev}—correlation coefficient of the validation, R^2_{ev}—correlation coefficient of calibration.

Predictions obtained from the Pt model are rather fair, even when external validation is applied (Table VI). There are only 3 molecules with relative errors between 10 and 15% (Fig. 6). As expected according to the parameters in Table V, the BDD model has several phenolics with relative errors above 10%: 4 phenolics with errors between 10 and 15%, 2 phenolics with errors between 15 and 20%, 1 phenolic with error above 20% (pAMI), and 1 phenolic compound with a large error of 60% (DOPA, Fig. 6). Both models show very similar prediction trends when externally validated. It is interesting to note that, even when four phenolics were used in the training sets during the external validation, the predictive power of the BDD model did not alter significantly. It can be concluded that the Pt

Table VI. Results for the QSPR model prediction capacities.

	Pt Model				BDD Model			
	Pred.[a]	Diff.[a]	EV Pred.[b]	EV Diff.[b]	Pred.[a]	Diff.[a]	EV Pred.[b]	EV Diff.[b]
PHEN	1.61	−0.06	1.59	−0.04	1.18	−0.11	1.19	−0.12
CATE[c]	1.36	−0.15	**1.37**	**−0.16**	1.05	−0.02	1.06	−0.03
RESO[c]	1.60	0.12	**1.59**	**0.13**	1.12	0.03	1.14	0.01
HYDR[d]	1.37	−0.01	1.37	−0.01	1.16	−0.11	**1.19**	**−0.14**
oAMI	1.24	0.08	1.25	0.07	1.15	0.11	1.17	0.09
pAMI	1.15	−0.14	1.16	−0.15	1.12	−0.21	1.14	−0.23
PARA[c]	1.43	0.01	**1.42**	**0.02**	1.06	0.05	1.06	0.05
oCRE	1.69	−0.06	1.68	−0.05	1.20	−0.04	1.22	−0.06
mCRE	1.65	0.06	1.64	0.07	1.17	0.17	1.16	0.18
pCRE	1.67	0.03	1.66	0.04	1.18	0.11	1.17	0.12
pCmC[d]	1.66	−0.06	1.65	−0.05	0.88	−0.09	**0.88**	**−0.09**
oCHL	1.69	0.04	1.68	0.05	0.98	−0.05	0.97	−0.04
oNIT[d]	1.79	−0.09	1.77	−0.07	1.00	0.09	**0.97**	**0.12**
GUAI	1.47	0.08	1.47	0.08	1.20	−0.01	1.19	0.00
CGUA	1.55	−0.02	1.56	−0.03	0.78	0.19	0.78	0.19
DOPA	1.18	−0.11	1.19	−0.12	0.77	−0.29	0.76	−0.28
LDOP	1.20	0.10	1.21	0.09	0.84	0.18	0.88	0.14
SERO[d]	1.29	0.11	1.30	0.10	1.13	0.01	**1.12**	**0.02**
HYIN	1.30	0.03	1.30	0.03	1.21	0.08	1.23	0.06
LTYR[c]	1.52	0.02	**1.50**	**0.04**	1.30	−0.07	1.31	−0.08
NORA[e]	1.15		1.17		0.88		0.87	
ADRE[e]	1.27		1.29		0.82		0.78	
mAMI[e]	1.46		1.44		1.12		1.13	
o'AoC[e]	1.47		1.47		−2.80		−2.48	
TYRA[e]	1.51		1.50		1.11		1.08	
mNIT[e]	1.65		1.64		1.02		1.00	
opDM[e]	1.69		1.68		1.14		1.14	
pCHL[e]	1.71		1.70		1.03		1.01	
opDC[e]	1.71		1.72		1.08		1.12	
pNIT[e]	1.73		1.71		1.03		1.03	

[a] Predictions obtained from the PLS models based on training sets with 20 phenolics: Pred.—prediction values of passivation, Diff.—difference between experimental and predicted values of passivation.
[b] Predictions obtained from the externally validated PLS models based on training sets with four phenolics: EV Pred.—prediction values of passivation, EV Diff.—difference between experimental and predicted values of passivation.
[c] Phenolics forming the external validation set for passivation on the Pt electrode. Corresponding predicted values and the differences are in bold.
[d] Phenolics forming the external validation set for passivation on the BDD electrode. Corresponding predicted values and the differences are in bold.
[e] Phenolics of the prediction set with corresponding values of passivation.

model is a parsimonius model with high predictive power, and yet recommended for practical purposes. However, the BDD model does not possess such predictive ability and cannot be recommended for prediction of phenolic passivation on the BDD electrode. This model can be rather useful for better understanding phenolic electropassivation at the BDD electrode. Equations 3 and 4 present the regression vectors for the final models in deautoscaled form

$$\log(\Delta j_{Pt}) = -5.918 - 0.514\text{HBD/N} + 0.072\text{Mor06u} + 2.368\text{Qcnpa} + 6.860\text{Ar} - 0.269\text{QNUnpa} \quad [3]$$

$$\log(\Delta j_{BDD}) = 1.955 - 8.404\text{DdC-O} - 0.015\text{DISPm} - 0.080\text{C-026} - 0.081\text{L(nCaH)} \quad [4]$$

Predictions for 10 phenolics (Fig. 4) are in Table VI. Both PLS models provide reasonable predictions even when externally validated, with the exception of the prediction for o'AoC for which the BDD model seriously fails. The validity of these predictions can be verified by comparing predictions and corresponding deviations for similar phenolics from the training and/or external validation sets. With respect to some phenolics that are under study in this work, the comparisons additionally confirm the reliability of the predictions in Table VI. Besides, predicted behavior of the 10 phenolics is mainly similar to that experimentally observed at other platinum or carbon electrodes.[55-61]

Molecular descriptors (Table II) make positive or negative contributions to the passivation at the Pt or BDD electrodes, which is easily noted from descriptor-passivation correlations (Table III), regression vectors (Table V), regression equations (Eq. 3 and 4), and especially from the exploratory analysis. Because of this fact, interpretation of the regression vectors has already been presented in the correlation and exploratory analyses. It can be concluded that both PLS models indicate more rigid and compact phenolic molecules, which more easily form polymeric films on the electrodes. This fact can be useful in predicting behavior of phenolics during electrooxidation, at both the qualitative and quantitative level.

Conclusions

Substituent effects largely determine the electropassivation processes at the Pt and BDD electrodes. The preference of radical attack to ortho, ortho′, meta, meta′, or para positions that are occupied with hydrogen or halogen atoms can be visualized by means of NPA partial atomic charges of the corresponding carbon atoms. The charges show whether the substitution site is electron rich or poor and, consequently, if the site should undergo electrophilic or nucleo-

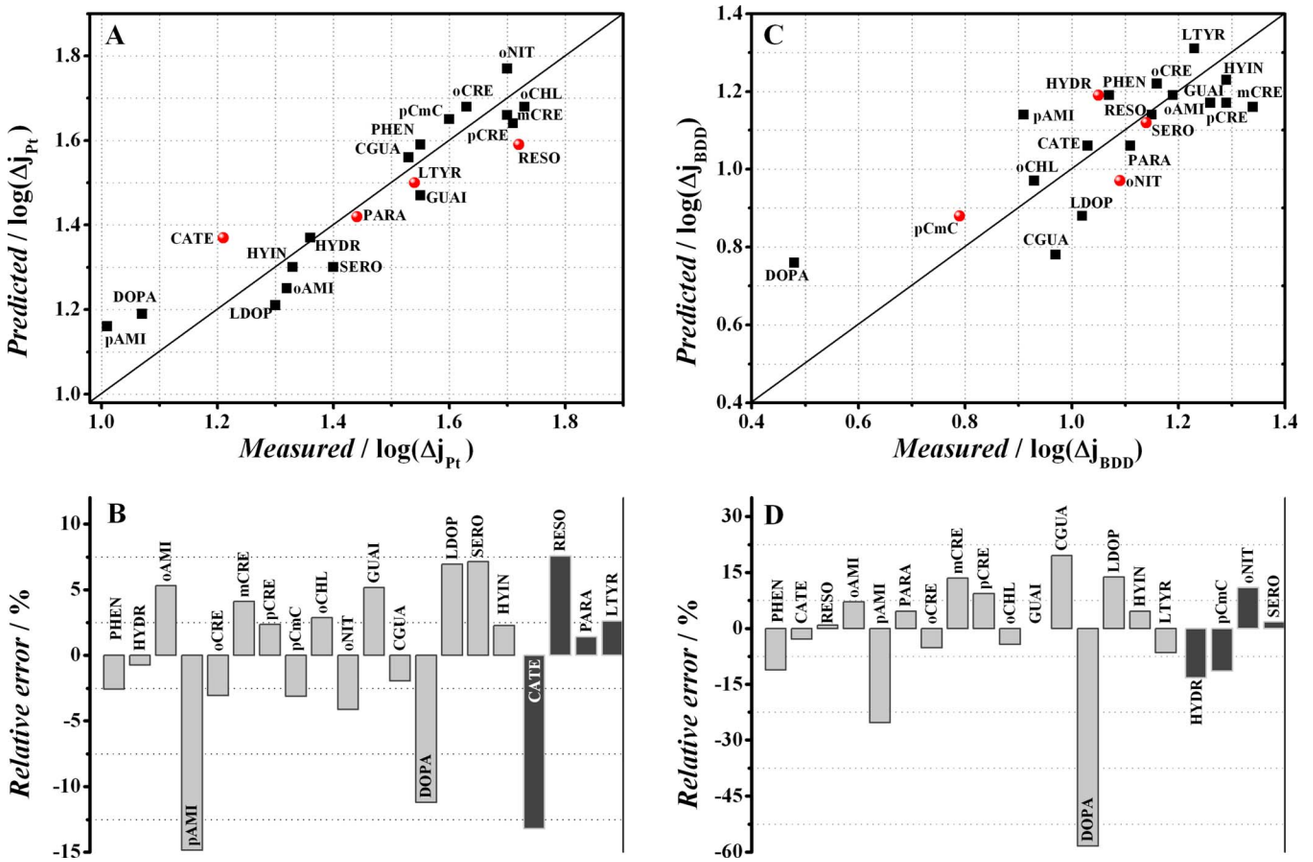

Figure 6. (Color online) Prediction capacity using PLS models (A–C) and relative error (B–D) for the Pt model and the BDD model, respectively. Key for graphics A and C: Predictions for calibration compounds (■); predictions for external compounds (●). Key for graphics B and D: light gray—relative error for calibration compounds; dark gray—relative error for external compounds.

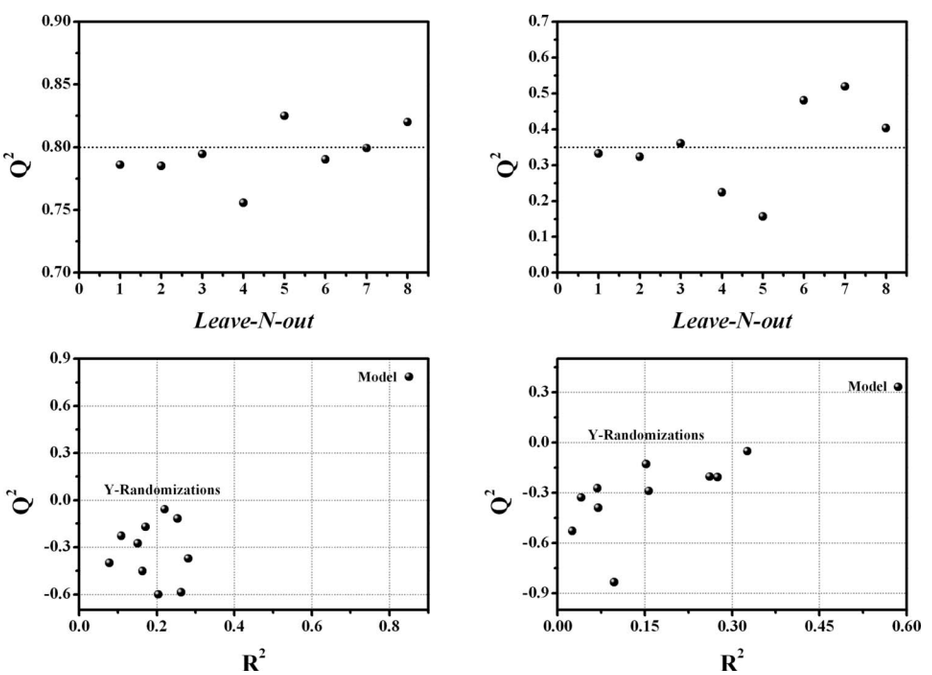

Figure 7. Validation of the Pt model (left images) and the BDD model (right images) by means of leave-*N*-out cross validation (upper images) and *Y*-randomization (lower images). Mean Q^2 values are shown by dashed lines for leave-*N*-out cross validation.

philic aromatic substitution, respectively. The classical organic chemistry approach in terms of resonance structures, which show inductive and resonance effects of the substituents, is a qualitative view of NPA charge distribution. In the absence of steric effects, this charge classification is a good aid in predicting phenoxyl radical formation.

Oxidation of phenolics into phenoxyl radicals results in higher reactivity of the new species. Phenolic electropassivation at the Pt electrode is satisfactorily described by the PLS model, which can be used for practical purposes. Although the PLS model for the phenolic passivation at the BDD electrode is far from being statistically relevant, it gives some idea about this phenomenon. Exploratory analysis makes it possible to understand which molecular features of phenolics are related to fouling of these compounds on the Pt and BDD electrodes.

This is the first time that phenolic passivation is treated at a quantitative level by means of QSPR analysis. Such studies could be expanded to other phenolic compounds and other electrodes. Such QSPR analyses may become routine in analytical laboratories that use phenols in electrochemical assays.

Acknowledgments

The authors acknowledge FAPESP and CNPq for financial support and Dr. Carol H. Collins for English revision.

Universidade Estadual de Campinas assisted in meeting the publication costs of this article.

References

1. W. I. Taylor and A. R. Battersby, *Oxidative Copling of Phenols*, Marcel Dekker, New York (1967).
2. J. Wang, M. Jiang, and F. Lu, *J. Electroanal. Chem.*, **444**, 127 (1998).
3. M. S. Ureta-Zanartu, P. Bustos, M. C. Diez, M. L. Mora, and C. Gutierrez, *Electrochim. Acta*, **46**, 2545 (2001).
4. M. Gattrell and D. W. Kirk, *J. Electrochem. Soc.*, **139**, 2736 (1992).
5. M. Gattrell and D. W. Kirk, *J. Electrochem. Soc.*, **140**, 903 (1993).
6. M. Gattrell and D. W. Kirk, *J. Electrochem. Soc.*, **140**, 1534 (1993).
7. Z. Ežerskis and Z. Jusys, *J. Appl. Electrochem.*, **31**, 1117 (2001).
8. V. Climent, A. Rodes, R. Albalat, J. Claret, J. M. Feliu, and A. Aldaz, *Langmuir*, **17**, 8260 (2001).
9. M. Ozden, E. Ekinci, and A. E. Karagozler, *J. Solid State Electrochem.*, **2**, 427 (1998).
10. M. S. Ureta-Zanartu, P. Bustos, C. Berrios, M. C. Diez, M. L. Mora, and C. Gutierrez, *Electrochim. Acta*, **47**, 2399 (2002).
11. H. J. Salavagione, J. Arias, P. Garces, E. Morallon, C. Barbero, and J. L. Vazquez, *J. Electroanal. Chem.*, **565**, 375 (2004).
12. D. Gonçalves, R. C. Faria, M. Yonashiro, and L. Bulhoes, *J. Electroanal. Chem.*, **487**, 90 (2000).
13. A. Guenbour, A. Kacemi, A. Benbachir, and L. Aries, *Prog. Org. Coat.*, **38**, 121 (2000).
14. A. Guenbour, A. Kacemi, and A. Benbachir, *Prog. Org. Coat.*, **39**, 151 (2000).
15. G. Mengoli and M. M. Musiani, *J. Electrochem. Soc.*, **134**, C643 (1987).
16. P. I. Iotov and S. V. Kalcheva, *J. Electroanal. Chem.*, **442**, 19 (1998).
17. Z. Ežerskis and Z. Jusys, *J. Appl. Electrochem.*, **32**, 543 (2002).
18. M. Karhu, *J. Chem. Soc., Perkin Trans. 1*, **1981**, 303.
19. R. S. Neves, A. J. Motheo, F. Fernandes, and R. Fartaria, *J. Braz. Chem. Soc.*, **15**, 224 (2004).
20. M. P. Soriaga and A. T. Hubbard, *J. Am. Chem. Soc.*, **104**, 2735 (1982).
21. V. Chia, M. P. Soriaga, and A. T. Hubbard, *J. Phys. Chem.*, **91**, 78 (1987).
22. F. Lu, G. N. Salaita, L. Laguren Davidson, D. A. Stern, E. Wellner, D. G. Frank, N. Batina, D. C. Zapien, N. Walton, and A. T. Hubbard, *Langmuir*, **4**, 637 (1988).
23. P. N. Bartlett, and J. M. Cooper, *J. Electroanal. Chem.*, **362**, 1 (1993).
24. L. V. Vasileva, I. V. Shchukin, and V. A. Babkin, *Russ. J. Electrochem.*, **29**, 609 (1993).
25. Y. Nishiki, T. Furuta, and T. Kurosu, *Electrochemistry (Tokyo, Jpn.)*, **72**, 521 (2004).
26. M. B. Smith and J. March, *March's Advanced Organic Chemistry: Reactions, Mechanisms and Structure*, 5th ed., John Wiley & Sons, New York (2001).
27. R. M. De Carvalho, L. T. Kubota, and S. Rath, *J. Electroanal. Chem.*, **548**, 19 (2003).
28. Z. Ežerskis, G. Stalnionis, and Z. Jusys, *J. Appl. Electrochem.*, **32**, 49 (2002).
29. D. R. Armstrong, C. Cameron, D. C. Nonhebel, and P. G. Perkins, *J. Chem. Soc., Perkin Trans. 2*, **1983**, 575.
30. M. M. C. Ferreira, *J. Braz. Chem. Soc.*, **13**, 742 (2002).
31. C. X. Xue, R. S. Zhang, H. X. Liu, X. J. Yao, M. C. Liu, Z. D. Hu, and B. T. Fan, *J. Chem. Inf. Comput. Sci.*, **44**, 669 (2004).
32. R. Bosque and J. Sales, *J. Chem. Inf. Comput. Sci.*, **43**, 637 (2003).
33. K. Nesmerak, I. Nernec, M. Sticha, K. Waisser, and K. Palat, *Electrochim. Acta*, **50**, 1431 (2005).
34. M. M. C. Ferreira, A. M. Antunes, M. S. Melgo, and P. L. O. Volpe, *Quim. Nova*, **22**, 724 (1999).
35. H. Martens and T. Naes, *Multivariate Calibration*, John Wiley & Sons, Hoboken, NJ (1989).
36. R. F. Teófilo, H. J. Ceragioli, A. C. Peterlevitz, L. M. Da Silva, F. S. Damos, M. M. C. Ferreira, V. Baranauskas, and L. T. Kubota, *J. Solid State Electrochem.*, **11**, 1449 (2007).
37. V. Baranauskas, A. C. Peterlevitz, H. J. Ceragioli, L. T. Kubota, and R. F. Teófilo, Brazil Pat. No. PI0600897-6 (2006).
38. M. C. Granger, M. Witek, J. S. Xu, J. Wang, M. Hupert, A. Hanks, M. D. Koppang, J. E. Butler, G. Lucazeau, M. Mermoux, et al., *Anal. Chem.*, **72**, 3793 (2000).
39. E. Mahe, D. Devilliers, and C. Comninellis, *Electrochim. Acta*, **50**, 2263 (2005).
40. R. L. McCreery, in *Laboratory Techniques in Electroanalytical Chemistry*, P. T. Kissinger and W. R. Heineman, Editors, p. 293, Marcel Dekker, New York (1996).
41. K. Štulík, *Electroanalysis*, **4**, 829 (1992).
42. F. H. Allen, *Acta Crystallogr., Sect. B: Struct. Sci.*, **58**, 380 (2002).
43. Cambridge Structural Database, version 5.28, with Jan. and May 2007 updates. Cambridge Structural Data Centre, University of Cambridge, Cambridge (2006).
44. I. J. Bruno, J. C. Cole, P. R. Edgington, M. Kessler, C. F. Macrae, P. McCabe, J. Pearson, and R. Taylor, *Acta Crystallogr., Sect. B: Struct. Sci.*, **58**, 389 (2002).
45. ConQuest, version 1.9, CSD searching software. Cambridge Structural Data Centre, University of Cambridge, Cambridge (2007).
46. Mercury, Version 1.5, Crystal Structure Viewer. Cambridge Structural Data Centre, University of Cambridge, Cambridge (2006).
47. WebLab ViewerPro, Version 4.0, High-Quality Molecular Visualization Software, Accelrys, Burlington (2000).
48. T. Ziegler, *Chem. Rev. (Washington, D.C.)*, **91**, 651 (1991).
49. A. D. Becke, *J. Chem. Phys.*, **98**, 5648 (1993).
50. C. T. Lee, W. T. Yang, and R. G. Parr, *Phys. Rev. B*, **37**, 785 (1988).
51. Titan, Version 1.0.8, Molecular Modeling Software. Wavefunction, Inc., Irvine (2001).
52. R. Todeschini, V. Consonni, A. Mauri, and M. Pavan, Dragon Web Version, Software for Calculation of Molecular Descriptors, Version 3.0. University of Milano, Bicocca (2003).
53. S. Wiklund, D. Nilsson, L. Eriksson, M. Sjostrom, S. Wold, and K. Faber, *J. Chemom.*, **21**, 427 (2007).
54. S. Wold and L. Eriksson, in *Chemometric Methods in Molecular Design*, H. Van de Waterbeemd, Editor, p. 309, VCH, Weinheim (1995).
55. Z. Ežerskis and Z. Jusys, *Pure Appl. Chem.*, **73**, 1929 (2001).
56. J. Wang, R. P. Deo, and M. Musameh, *Electroanalysis*, **15**, 1830 (2003).
57. B. Hoyer and N. Jensen, *J. Electroanal. Chem.*, **601**, 153 (2007).
58. J. M. Zen, H. H. Chung, H. H. Yang, M. H. Chiu, and J. W. Sue, *Anal. Chem.*, **75**, 7020 (2003).
59. R. Gonzalez, A. Sanchez, M. Chicharro, M. D. Rubianes, and G. A. Rivas, *Electroanalysis*, **16**, 1244 (2004).
60. X. Yao, H. Wu, J. Wang, S. Qu, and G. Chen, *Chem.-Eur. J.*, **13**, 846 (2007).
61. H. Keles and I. Dehri, *Appl. Surf. Sci.*, **252**, 7545 (2006).
62. Matlab—The Language of Technical Computing, version 7.0. Mathworks, Natick (2004).
63. Pirouette—Multivariate Data Analysis Software, Version 3.02. Infometrix, Woodinville (2001).
64. S. Alehashem, F. Chambers, J. W. Strojek, G. M. Swain, and R. Ramesham, *Anal. Chem.*, **67**, 2812 (1995).
65. G. W. Muna, N. Tasheva, and G. M. Swain, *Environ. Sci. Technol.*, **38**, 3674 (2004).
66. B. V. Sarada, T. N. Rao, D. A. Tryk, and A. Fujishima, *Anal. Chem.*, **72**, 1632 (2000).
67. R. Kiralj and M. Ferreira, *J. Chem. Inf. Comput. Sci.*, **42**, 508 (2002).
68. R. T. Morrison and R. N. Boyd, *Organic Chemistry*, 3rd ed., Allyn and Bacon, Boston (1981).
69. M. Ferreira, H. Varela, R. M. Torresi, and G. Tremiliosi, *Electrochim. Acta*, **52**, 434 (2006).
70. C. C. Chang, L. C. Chen, S. J. Liu, and H. C. Chang, *J. Phys. Chem. B*, **110**, 19426 (2006).
71. A. Tropsha, P. Gramatica, and V. K. Gombar, *QSAR Comb. Sci.*, **22**, 69 (2003).
72. A. Golbraikh and A. Tropsha, *J. Mol. Graphics Modell.*, **20**, 269 (2002).